Reports

Fabrication and Use of Nanometer-Sized Electrodes in Electrochemistry

REGINALD M. PENNER, MICHAEL J. HEBEN, TERESA L. LONGIN, NATHAN S. LEWIS*

Electrodes with electrochemical dimensions as small as 10 angstroms have been fabricated and used for electrochemical studies. These nanometer-scale electrodes have enabled the measurement of electron-transfer rate constants, k_{het}, that are two orders of magnitude faster than k_{het} values accessible with any other electrochemical method.

ULTRASMALL ELECTRODES ARE being increasingly used in areas as diverse as scanning tunneling microscopy (STM) (*1*), electrophysiology (*2*), chemical kinetics (*3*), and nanolithography (*4*). The temporal and spatial advantages of small electrodes have allowed electrochemists to measure the rates of fast chemical reactions (*3, 5, 6*), to perform in vivo voltammetric measurements inside living brain tissue (*7*) and inside single cells (*8*), to observe changes in the conductivity of single ion channels (*9*), to efficiently detect analytes eluted from a capillary zone electrophoresis column (*10*), and to perform small-scale etching and lithography (*4*). In all of these applications, the performance of the electrode with respect to speed and spatial resolution scales inversely with the electrode radius. Microband electrodes with lateral dimensions as small as 20 Å have been reported previously (*11*), but the large longitudinal dimension of these electrodes (1 to 10 mm) precludes their application to small-scale lithography, STM, neurophysiology, and to electrochemical experiments that require the achievement of steady-state current densities. Ultramicroelectrodes with the smallest maximum dimension reported to date have an exposed radius of 0.1 μm (*12*), and more typical sizes are in the range 1.0 to 10.0 μm. In this report we describe a method that has allowed the routine fabrication of electrodes with electrochemical radii as small as 10 Å. We also describe the use of these nanometer-scale electrodes (nanodes) to determine electron-transfer rate constants that are two orders of magnitude faster than those accessible with any other currently available electrochemical method.

Division of Chemistry and Chemical Engineering, California Institute of Technology, Pasadena, CA 91125.

*To whom correspondence should be addressed.

The nanodes were fabricated in a two-step procedure. We sharpened 0.50-mm diameter Pt or Pt-Ir (70:30) wire electrochemically with an ac etching procedure, as described previously (*13, 14*). Etched wires were then translated at 0.10 mm/s through a molten glass bead that was held in a resistively heated, circular Pt filament (inside diameter ≈ 2 mm). The size of the aperture in the resultant glass coating was related to the translation velocity and to the temperature of the molten glass: at a constant wire-translation velocity, the effective aperture radius r increased with increasing insulator melt temperature (*13, 14*). Temperatures in the range 1250° to 1370°C were maintained to prepare electrodes with radii of 10 Å to 20 μm. Precise control over the temperature and translation velocity was required in order to fabricate the smallest aperture structures; small adjustments in melt temperature (10°C) and tip velocity (0.01 mm/s) were performed iteratively in order to obtain electrodes in a desired size regime. This two-step etching and coating process closely resembles standard procedures used to prepare glass-coated Pt electrodes 1 to 50 μm in diameter for neurophysiology applications (*15*), except that the refinements in procedure described above yielded electrodes with much smaller exposed metal areas. Iterative control of the relation between glass melt temperature and r readily enabled the fabrication of small apertures in high yield: ~50% of the electrodes fabricated had radii of <0.10 μm (see above), and approximately 10% (out of more than 200 electrodes fabricated in our laboratory) exhibited apparent electrochemical radii in the range from 10 to 100 Å.

Scanning electron microscope (SEM) images of the larger radii (≥0.5 μm) electrodes showed exposed metal apertures of dimensions that were in agreement with the electrochemically determined electrode radius (*14*). In contrast, the smallest aperture nanodes appeared to be completely covered with glass even at the highest magnifications available with the SEM (×50,000). However, these structures were not totally insulating when used as electrodes, but exhibited conventional steady-state microelectrode behavior. The voltammetry of representative nanodes in several electrolytes containing redox active ions is shown in Fig. 1. The mass-transport–controlled limiting current,

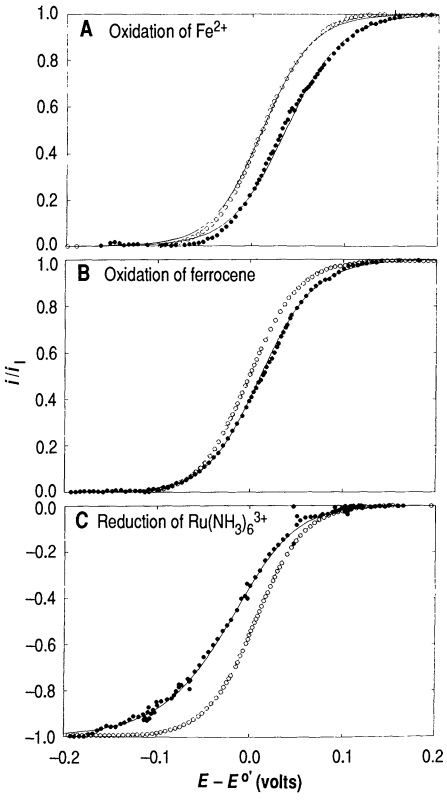

Fig. 1. Voltammetric response (5 mV/s) of several nanodes in various electrolytes: (**A**) 0.1 H_2SO_4, H_2O; (**B**) 0.3 M $(C_4H_9)_4NClO_4$, CH_3CN; and (**C**) 0.5 M KCl, H_2O. Each voltammogram was normalized to the value of i_l after subtraction of a sloping baseline. Concentrations of redox species and experimental conditions were as follows: (A) (○) 6.67 mM, i_l = 49 nA, r = 17 μ, k_{het} = 0.014 cm/s, and (●) 6.51 mM, i_l = 5.3 nA, r = 1.9 μm, k_{het} = 0.017 cm/s; (B) (○) 4.30 mM, i_l = 19 nA, r = 3.0 μm, and (●) 2.97 mM, i_l = 6.8 pA, r = 16 Å, k_{het} = 220 cm/s; and (C) (○) 3.54 mM, i_l = −7.3 nA, r = 4.2 μm, and (●) 3.45 mM, i_l = −1.9 pA, r = 11 Å, k_{het} = 47 cm/s. In (B) and (C), the fit to the open-circle data was unchanged for all electrodes with radii >50 Å and was in excellent agreement with the Nernstian behavior (dashed line) generated by using the value of $E^{o'}$ obtained from voltammetric measurements at the largest nanode radii. In (A), the Nernstian voltammogram (dashed line) was determined by measurement of $E^{o'}$ using cyclic voltammetry, because k_{het} for $Fe^{3+/2+}$ is so small that kinetic voltammograms were obtained even at the largest microelectrodes used in this work. The deviations observed from ideal Nernstian behavior allow determination of k_{het}.

i_l, measured from the plateau region of the sigmoidal steady-state voltammogram, can be related to the effective electrochemical radius of exposed metal by Eq. 1 (*16*):

$$i_l = 2\pi nFDC^*r_{app} \quad (1)$$

where F is Faraday's constant, n is the number of electrons transferred in the reaction, D is the diffusion coefficient of the reactant (centimeters squared per second), C^* is the bulk concentration of the reactant (moles per cubic centimeter), and r_{app} is the apparent electrochemical radius (centimeters). In the absence of direct observations of the geometry of the aperture, Eq. 1 can be used within conventional diffusion theory to characterize empirically the apparent electrochemical radius of the aperture. We used Eq. 1 to calculate electrochemical radii of 1.9 and 17.4 μm for the electrodes in Fig. 1A and of 16 Å and 3.0 μm for the electrodes in Fig. 1B. To validate this calculation, several (>10) nanodes were measured in one electrolyte and were then transferred to a solution containing a different redox couple; agreement between the calculated r values in these independent measurements was typically within 20%. A tacit assumption implied in the use of Eq. 1 is that the electrode has a hemispherical geometry. The assumption of other exposed metal geometries (such as a disk or a cone) would yield apparent electrode radii that would be 20 to 30% larger than those obtained from Eq. 1 [the factor 2π would be replaced by 4.0 for a disk (*17*) and by $\sim 2\pi$ for a cone (*14*)], but this does not affect the primary conclusion that extremely small electrodes have been prepared by the etching-coating method.

Although the absolute magnitude of the current for these nanodes is small, the effective current densities are extremely large. The 70 A/cm^2 current density calculated for the nanode in Fig. 1C exceeds by two orders of magnitude the current densities accessible in this electrolyte with a rotating-disk electrode or with ac-potential modulation methods (*18*), and corresponds to a mass-transport velocity $m_0 (= D/r_{app})$ of 100 cm/s. The large m_0 values generated by nanodes extends the range of maximum measurable electron-transfer rate constants (k_{het}), because the rate of electron transfer is less likely to be limited by mass transport of the reactant to the electrode surface. Smaller electrodes are advantageous because the current density is inversely related to the electrode radius, implying that the maximum measurable value of k_{het} increases linearly with $1/r$. Microelectrodes that display steady-state currents are also desirable because the extraction of kinetic information from steady-state voltammograms does not require correction for resistance and capacitance effects or the construction of extremely high speed (>megahertz) potentiostats (*19*). Nanodes with $r_{app} \sim 10$ Å described in this report are capable of measuring k_{het} values that are within a factor of 6 of the values attainable with a hypothetical single Pt atom ($r = 1.53$ Å) as an electrode.

The complete steady-state voltammetry for a collection of different nanodes in contact with a variety of electrolytes is shown in Fig. 1. As expected, when the apparent electrode radius was sufficiently large ($r >> D/k_{het}$), mass-transport–limited (that is, Nernstian) electrode behavior was observed, and the peak shape and position on the potential axis was independent of further increases in electrode radius (dashed curves, Fig. 1). No quantitative kinetic information can be obtained from such voltammetric data.

In contrast, when the electrode radius becomes comparable to the value of D/k_{het} (*20*), mass transport is sufficiently rapid that the wave shape is no longer independent of electrode radius, and k_{het} can be determined from an analysis of the voltammogram shape and its position on the potential axis (*20, 21*). The exact equations for calculating kinetic voltammograms at microelectrodes have been derived by Zoski and Oldham (*22*), and we have used this theory to extract values of k_{het} and α from the steady-state nanode data. The magnitude of the potential shift at the formal potential $E^{\circ\prime}$ was used to evaluate k_{het}, and the slope of $\ln(k_{het})$ versus $E^{\circ\prime}$ in the potential interval ± 10 mV of $E^{\circ\prime}$ was used to evaluate the value of the transfer coefficient, α (*22*). Best-fit voltammograms obtained by this procedure are displayed as solid lines through the experimental data in Fig. 1. The fit of the calculated I-V curve to the experimental data was not very sensitive to α, which ranged from 0.5 to 0.7. Values of the heterogeneous rate constants obtained for the three redox couples depicted in Fig. 1 and for the other redox couples investigated in this work are summarized in Table 1.

Kinetic parameters for relatively slow electron-transfer reactions ($k_{het} < 0.5$ cm/s) have been measured previously with conventional electrochemical methods. Our measuremets of two k_{het} values reported to be in the range $k_{het} = 10^{-3}$ to 10^{-1} cm/s were in good agreement with those of previous workers (Table 1). In these measurements electrodes were used with electrochemical radii at the large end of the range used in our work: Pt-Ir electrodes with apparent radii of 1.0 to 2.0 μm were sufficient to measure k_{het} for $Ru(NH_3)_6^{3+/2+}$ in 50 mM KPF_6(aq) and k_{het} for $Fe^{3+/2+}$ in 0.1 M H_2SO_4(aq). Weaver and co-workers (*23*) have observed dramatic increases in k_{het} for cobalt amine complexes in aqueous electrolytes containing Cl^-; however, the magnitude of this effect for $Ru(NH_3)_6^{3+/2+}$ could not be quantified because k_{het} in 0.5 M KCl(aq) is too large to be measured by conventional techniques (*24*). In contrast to the kinetic data of Fig. 1A (obtained with a 1.9-μm apparent radius electrode), substantially smaller electrodes were required to observe kinetic voltammograms in $Ru(NH_3)_6^{3+/2+}$ solutions containing 0.5 M KCl. Kinetic voltammograms were obtained with Pt nanodes that had $r_{app} = 10$ to 20 Å, and these data yielded a value for k_{het} of 79 ± 44 cm/s (Fig. 1 and Table 1). A lower limit for k_{het} for ferrocene$^{+/0}$ ($Fc^{+/0}$) of > 6 cm/s has been estimated by Bond *et al.* (*25*) from steady-state voltammetry at microelectrodes with $r_{app} = 0.3$ μm. Our measurements at Pt nanodes with $r_{app} = 15$ to 20 Å yield a value for k_{het} of 220 ± 120 cm/s in CH_3CN, 0.10 M Bu_4NClO_4 electrolyte (Bu, n-C_4H_9). In contrast to $Ru(NH_3)_6^{3+/2+}$ and $Fc^{+/0}$, both methyl viologen$^{2+/+}$ ($MV^{2+/+}$) and 1,1′-dicarbomethoxycobaltocene$^{+/0}$ ($Cp^{\#}{}_2Co^{+/0}$) exhibited reversible voltammetric behavior even at nanodes with $r_{app} \approx 20$ Å, indicating that $k_{het} > 170 \pm 90$ cm/s for $MV^{2+/+}$ and $k_{het} > 130 \pm 70$ cm/s for $Cp^{\#}{}_2Co^{+/0}$. These data are useful because the Nernstian response observed at the smallest electrodes indicates that the kinetic voltammetry obtained for other systems at $r_{app} = 10$ to 50 Å nanodes is unlikely to be an artifact resulting from unusual voltammetric responses at nanometer-sized electrodes. No evidence for a dependence of k_{het} on the electrode dimension was observed for the electrolyte concentrations and r_{app} values used in this work (*26*).

Another assumption implicit in the present analysis is that the electrodes consisted only of a single aperture, as opposed to many interconnected, smaller radius, metallic regions with isolated diffusion layers. This latter scenario would lead to an underestimate of the true rate constant, because the true electrochemical radius of each individual domain would be smaller than r_{app} determined from the observed limiting current by using Eq. 1. For the 0.1- to 10-μm electrodes, the agreement between k_{het} values obtained in this work and values independently determined by other methods indicates that errors arising from a predominance of small radius features are not substantial for nanodes with $r_{app} \approx 0.1$ to 10 μm. For measurements with nanodes with $r_{app} = 100$ to 1000 Å, the rate data could in principle yield an underestimate of the true k_{het} value. However, the redox couples in Table 1 that exhibited fast elec-

trode kinetics only displayed measurable voltammetric shifts at the smallest apparent radii nanodes (r_{app} = 10 to 20 Å), where the possible systematic underestimate in k_{het} due to a distribution of interconnected metallic domains with even smaller radius would be only a factor of 2 if all of the isolated domains were three atoms in diameter (8 Å diameter). Another consideration is that at the smallest electrode radii ($r \approx 10$ to 20 Å) corrections for double-layer effects, for possible finite-size effects of the ions and of the diffusion layer (*12, 26*), and for migration effects might yield important differences between the true rate constants and those obtained above from a classical electrochemical analysis. These effects are expected to diminish greatly with increases in the electrode size; thus, the lack of a kinetic shift in the voltammetry at $r_{app} \approx 100$ Å nanodes suffices to provide important information on lower limits for the rate constants for the $Fc^{+/0}$, $MV^{2+/+}$, and $Ru(NH_3)_6^{3+/2+}$ KCl redox systems, and serves to establish the usefulness of nanode voltammetry in estimating heterogeneous rate constants for such rapid redox couples. A quantitative assessment of the effects of finite ion size or a finite diffusion-layer thickness or both could also be addressed in principle with these nanodes, if an independent measure of the exposed electrode aperture can be obtained.

The k_{het} values determined by application of these classical electrochemical kinetic equations are in good agreement with expectations based on electron-transfer theories. Marcus (*27*) has derived a relation between homogeneous self-exchange electron-transfer rate constants (k_{ex}) and heterogeneous rate constants:

$$k_{het} = Z_{het}(k_{ex}/Z_{bi})^{1/2} \quad (2)$$

where Z_{bi} is the bimolecular collision frequency, 10^{11} M^{-1} s^{-1}, and Z_{het} is the unimolecular collision frequency into a surface, 10^4 cm/s. The validity of this relation was questioned by earlier heterogeneous kinetic measurements (*28*) that were later disputed as being limited by the time response of the technique. The self-exchange rates (k_{ex}) for $Fe^{3+/2+}$ [~3 M^{-1} s^{-1} (*29, 30*)] and $Ru(NH_3)_6^{3+/2+}$ [~4×10^3 M^{-1} s^{-1} (*31, 32*)] can be used in Eq. 2 to predict k_{het} values of 0.05 and 2 cm/s, respectively, which are in reasonable agreement with the experimental values obtained in this work and measured previously (Table 1). Similarly, k_{ex} for $Fc^{+/0}$ [8.5×10^6 M^{-1} s^{-1} (*33*)] corresponds to k_{het} = 90 cm/s and k_{ex} for $Cp^{\#}{}_2Co^{+/0}$ [1.9×10^8 M^{-1} s^{-1} (*34*)] yields a value for k_{het} of >400 cm/s, which is consistent with the observed voltammetric behavior. The indirect estimates of k_{ex} for $MV^{2+/+}$ [$k_{ex} = 8.0 \times 10^6$ M^{-1} s^{-1} (*35*)] predict a k_{het} of 90 cm/s, which is somewhat smaller than the lower limit of 170 ± 90 cm/s that we report here.

Although the overall consistency of Eq. 2 is indicated by these new k_{het} measurements, more kinetic data is required to quantitatively test its validity under a variety of conditions. We note, however, that self-exchange kinetic measurements for most outer-sphere redox ions predict k_{het} values that are too large to measure with conventional methods but that can now be estimated with the use of nanodes and the steady-state voltammetric method described above. Nanometer-sized electrodes can be reproducibly fabricated and used to obtain heretofore unavailable kinetic information on a range of redox couples. Additionally, they should find application in a variety of areas, including neurophysiology, lithography, chemical analysis, and STM, and should help advance the methodology to construct and modify physical and chemical structures on a molecular scale.

Table 1. Measured k_{het} data, comparison with literature values of k_{het}, and comparison with k_{het} values calculated from Eq. 2 with literature values of k_{ex}. The r_{app} values were calculated from the measured limiting current i_l with Eq. 1. The ΔE values are shifts in the potential of the steady-state voltammogram relative to $E^{o\prime}$ at a reversible (Nernstian) voltammogram. Tabulated are the observed shifts for four electrodes of various sizes. The average k_{het} value and 1σ standard deviations listed are statistics for larger data sets of up to ten measurements.

r_{app}	ΔE (mV)	k_{het}* (cm s^{-1})	k_{het} (lit)† (cm s^{-1})	k_{ex} (lit)‡ (M^{-1} s^{-1})	k_{het} (calc)§ (cm s^{-1})
		$Fe^{3+/2+}$ (0.1 M H_2SO_4, H_2O)			
18 μm	10	0.018			
8.1 μm	14	0.022			
2.0 μm	30	0.031			
1.3 μm	44	0.029			
		0.018 ± 0.007	0.0032–0.018 (*20, 36, 37*)	1.1, 4.2	0.033, 0.065 (*28, 29*)
		$Ru(NH_3)_6^{3+/2+}$ (50 mM KPF_6, H_2O)			
4.6 μm	6	0.10			
3.7 μm	6	0.12			
1.6 μm	4	0.38			
1.3 μm	10	0.17			
		0.26 ± 0.13	0.35, 0.45 (*5, 23*)	3200, 4300	1.8, 2.5 (*30, 31*)
		$Ru(NH_3)_6^{3+/2+}$ (0.5 M KCl, H_2O)			
1.1 μm	0	>0.13			
269 Å	0	>9.3			
203 Å	0	>11			
11 Å	37	47			
		79 ± 44			
		$Fc^{+/0}$ (0.3 M Bu_4NClO_4, CH_3CN)			
2.6 μm	0	>0.22			
0.57 μm	0	>1.1			
18 Å	28	120			
16 Å	17	220			
		220 ± 120	0.7–3.1 (*5, 28, 38*)	8.5×10^6	90 (*33*)
		$MV^{2+/+}$ (0.1 M Bu_4NClO_4, CH_3CN)			
0.21 μm	0	>1.8			
0.11 μm	0	>3.6			
67 Å	0	>58			
22 Å	0	>170			
		>170 ± 90		8.0×10^6	90 (*35*)
		$(CpCOOCH_3)_2Co^{+/0}$(0.1 M Bu_4NClO_4, CH_3CN)			
4.7 μm	0	>0.066			
280 Å	0	>10			
37 Å	0	>77			
23 Å	0	>130			
		>130 ± 70		1.9×10^8‖	430 (*34*)

*Heterogeneous electron-transfer rate constants (uncorrected for double-layer effects) as measured with steady-state voltammetry. For electrodes that exhibited no potential shift, a lower limit of k_{het} is listed. In such cases, the lower limit was estimated as the value of k_{het} required to induce a 10-mV shift at $E^{o\prime}$. †Values of k_{het} reported in previously published work. ‡Electron self-exchange rate constants reported in previously published work. §Values for k_{het} calculated from k_{hex} using the Marcus cross-relation, Eq. 2. ‖Self-exchange rate for unsubstituted $CoCp_2^{+/0}$.

REFERENCES AND NOTES

1. R. Sonnenfeld and B. C. Schardt, *Appl. Phys. Lett.* **49**, 1172 (1986); P. Lustenberger, H. Rohrer, R. Christoph, H. Siegenthaler, *J. Electroanal. Chem.* **243**, 225 (1988); M. J. Heben, R. M. Penner, N. S. Lewis, M. M. Dovek, C. F. Quate, *Appl. Phys. Lett.* **54**, 1421 (1989).
2. A. M. Mamoon, W. T. Schlapfer, B. H. Fahwiler, C. A. Tobias, *Adv. Biol. Med. Phys.* **16**, 1 (1977); B. Sackmann and E. Neher, *Annu. Rev. Physiol.* **46**, 455 (1984).
3. A. Fitch and D. H. Evans, *J. Electroanal. Chem.* **202**, 83 (1986); W. J. Bower, E. E. Engelman, D. H. Evans, *ibid.* **262**, 67 (1989); C. P. Andrieux, P. Hapiot, J. M. Saveant, *J. Phys. Chem.* **92**, 5987 (1988); *ibid.*, p. 5992.
4. C. W. Lin, F. R. Fan, A. J. Bard, *J. Electrochem. Soc.* **134**, 1038 (1987); D. H. Craston, S. W. Lin, A. J. Bard, *ibid.* **135**, 785 (1988); J. Schneir *et al.*, *Proc. SPIE* **897**, 16 (1988).
5. D. O. Wipf, E. W. Kristensen, M. R. Deakin, R. M. Wightman, *Anal. Chem.* **60**, 306 (1988).
6. D. O. Wipf and R. M. Wightman, *ibid.*, p. 2460; C. P. Andrieux, D. Garreau, P. Happiot, J. Pinson, J. M. Saveant, *J. Electroanal. Chem.* **243**, 321 (1988).
7. P. T. Kissinger, J. B. Hart, R. N. Adams, *Brain Res.* **55**, 209 (1973); J. C. Conti, E. Strope, R. N. Adams, C. A. Marsden, *Life Sci.* **23**, 2705 (1978); A. G. Ewing, R. M. Wightman, M. A. Dayton, *Brain Res.* **249**, 361 (1982).
8. K. Tanaka and N. Kashiwagi, *Bioelectrochem. Bioenerg.* **17**, 519 (1987); *ibid.* **21**, 95 (1989).
9. E. Neher and B. Sackman, *Nature* **260**, 779 (1976); ———, J. H. Steinbach, *Pfluegers Arch. Gesamte Physiol. Menschen Tiere* **375**, 219 (1978); F. Conti and E. Neher, *Nature* **285**, 140 (1980).
10. R. A. Wallingford and A. G. Ewing, *Anal. Chem.* **60**, 1972 (1988); *ibid.*, p. 258.
11. J. Duke, E. R. Scott, H. S. White, *J. Electroanal. Chem.* **264**, 281 (1989).
12. M. Fleischmann, S. Pons, D. R. Rolison, P. P. Schmidt, *Ultramicroelectrodes* (Datatech Systems, Morgantown, NC, 1987), chap. 3.
13. M. J. Heben, M. M. Dovek, N. S. Lewis, R. M. Penner, C. F. Quate, *J. Microsc.* **152**, 651 (1988); M. J. Heben, thesis, California Institute of Technology (1990).
14. R. M. Penner, M. J. Heben, N. S. Lewis, *Anal. Chem.* **61**, 1630 (1989).
15. M. L. Wolbarsht, E. F. MacNichol, Jr., H. G. Wagner, *Science* **132**, 1309 (1960); C. Guld, *Med. Electron. Biol. Eng.* **2**, 317 (1964).
16. W. H. Reinmuth, *J. Am. Chem. Soc.* **79**, 6358 (1957).
17. M. A. Dayton, J. C. Brown, K. J. Stutts, R. M. Wightman, *Anal. Chem.* **52**, 946 (1980).
18. A. J. Bard and L. R. Faulkner, *Electrochemical Methods* (Wiley, New York, 1980), chaps. 5, 6, 8, and 9.
19. Experimental problems associated with the determination of k_{het} with cyclic voltammetry, for example, are discussed in the following references: D. F. Milner and M. J. Weaver, *Anal. Chem. Acta* **198**, 245 (1987); J. O. Howell, W. G. Kuhr, R. E. Ensman, R. M. Wightman, *J. Electroanal. Chem.* **209**, 77 (1986); A. M. Bond *et al.*, *Anal. Chem.* **60**, 1878 (1988).
20. A. Russell *et al.*, *Anal. Chem.* **58**, 2961 (1986); K. B. Oldham, C. G. Zoski, A. M. Bond, D. A. Sweigart, *J. Electroanal. Chem.* **248**, 467 (1988).
21. Z. Galus, J. Golas, J. Osteryoung, *J. Phys. Chem.* **92**, 1103 (1988).
22. K. B. Oldham and C. G. Zoski, *J. Electroanal. Chem.* **256**, 11 (1988).
23. M. J. Weaver and T. L. Satterberg, *J. Phys. Chem.* **81**, 1772 (1977); M. J. Weaver, *J. Electroanal. Chem.* **93**, 231 (1978); T. L. Satterberg and M. J. Weaver, *J. Phys. Chem.* **82**, 1784 (1978); S. W. Barr, K. L. Guyer, M. J. Weaver, *J. Electroanal. Chem.* **111**, 41 (1980).
24. T. Gennett and M. J. Weaver, *Anal. Chem.* **56**, 1444 (1984).
25. A. M. Bond *et al.*, *ibid.* **60**, 1878 (1988).
26. R. B. Morris, D. J. Franta, H. S. White, *J. Phys. Chem.* **91**, 3559 (1987).
27. R. A. Marcus, *ibid.* **67**, 853 (1963); R. A. Marcus, *Annu. Rev. Phys. Chem.* **15**, 155 (1964).
28. T. Saji, T. Yamada, S. Aoyagui, *J. Electroanal. Chem.* **61**, 147 (1975); T. Saji, *ibid.* **86**, 219 (1978).
29. J. Silverman and R. W. Dodson, *J. Phys. Chem.* **56**, 846 (1952).
30. B. S. Brunschwig, C. Creutz, D. H. Macartney, T. K. Sham, N. Sutin, *Faraday Discuss. Chem. Soc.* **74**, 113 (1982).
31. J. T. Hupp and M. J. Weaver, *J. Phys. Chem.* **93**, 4703 (1989).
32. T. J. Meyer and H. Taube, *Inorg. Chem.* **7**, 2369 (1968).
33. R. M. Neilson, G. E. McMannis, L. K. Safford, M. J. Weaver, *J. Phys. Chem.* **93**, 2152 (1989).
34. R. M. Neilson, G. E. McMannis, M. J. Weaver, *ibid.*, p. 4703.
35. C. R. Bock *et al.*, *Chem. Phys. Lett.* **61**, 522 (1979).
36. Z. Samec and J. Weber, *J. Electroanal. Chem.* **77**, 163 (1977).
37. D. H. Angell and T. Dickinson, *ibid.* **35**, 55 (1972).
38. M. I. Montenegro and D. Pletcher, *ibid.* **200**, 371 (1986).
39. We acknowledge the Office of Naval Research for support of this work and F. C. Anson and M. J. Weaver for helpful discussions. Contribution no. 8153 from the Division of Chemistry and Chemical Engineering at Caltech. We dedicate this report to George McManis, whose promising scientific career was tragically cut short by his untimely death.

15 August 1990; accepted 13 September 1990

Simulations of the Folding of a Globular Protein

JEFFREY SKOLNICK AND ANDRZEJ KOLINSKI

Dynamic Monte Carlo simulations of the folding of a globular protein, apoplastocyanin, have been undertaken in the context of a new lattice model of proteins that includes both side chains and α-carbon backbone atoms and that can approximate native conformations at the level of 2 angstroms (root mean square) or better. Starting from random-coil unfolded states, the model apoplastocyanin was folded to a native conformation that is topologically similar to the real protein. The present simulations used a marginal propensity for local secondary structure consistent with but by no means enforcing the native conformation and a full hydrophobicity scale in which any nonbonded pair of side chains could interact. These molecules folded through a punctuated on-site mechanism of assembly where folding initiated at or near one of the turns ultimately found in the native conformation. Thus these simulations represent a partial solution to the globular-protein folding problem.

THE SOLUTION TO THE PROTEIN folding problem should not only provide the folded native conformation of a protein, but also information on the mechanism by which a protein attains the folded configuration (*1–3*). Proteins do not fold by a random search (*3*). The observed folding times are on the order of seconds or minutes (*1, 4*), and a random search of all configurations by a small protein of 100 residues would take at least 10^{50} years (*3*). Unfortunately, because of the size of proteins and the time scale of folding, simplified models must be used to make the folding algorithms practical. One such simplification is to use a lattice (*5*). We describe results on a new class of lattice models applied to the folding, from randomly generated, unfolded conformations, of a 99-residue Greek key β-barrel protein, apoplastocyanin (*6*). The native structure is topologically similar to the nuclear magnetic resonance (NMR) solution structure of french bean Cu(I) plastocyanin (*7*) and the x-ray crystal structure of apopoplar plastocyanin (*8*), and differs only in local detail because of the small side-chain representation used in this preliminary study.

Lattice representations of proteins have a long history (*5, 9*). Recently Dill and coworkers (*10, 11*) exhaustively searched the sequence and conformational space of compact polymers and found that compactness induces secondary structure. These studies are complementary to the present work, which allows the examination of longer and more realistic chains, and where folding-pathway information is also obtained. However, the more realistic approach precludes an exhaustive sequence and conformational search.

For highly simplified diamond lattice models, we addressed the requirements to uniquely obtain the native state for model α-helical (*12*) and β-sheet proteins (*13, 14*) and also examined their folding pathways (*15, 16*). While a diamond lattice can perhaps provide general insights into the folding process, it poorly represents local secondary structures. Thus a different lattice must be used if proteins are to be treated in greater detail.

The new lattice model of globular proteins provides a good local description of the protein backbone conformation and yet remains computationally tractable. The entire space is embedded into an underlying cubic lattice where adjacent lattice sites are a dis-

J. Skolnick, Department of Molecular Biology, Research Institute of Scripps Clinic, La Jolla, CA 92037.
A. Kolinski, Department of Chemistry, University of Warsaw, 02-093 Warsaw, Poland.